Online Estimation and Compensation of Back-Electromotive Forces for Synchronous Reluctance Machine

Laurent Schuller, Romain Delpoux, Jean-Yves Gauthier, Xavier Brun

Online Estimation and Compensation of Back-Electromotive Forces for Synchronous Reluctance Machine

Laurent Schuller* *IEEE Student Member*, Romain Delpoux †, Jean-Yves Gauthier ‡ and Xavier Brun§
Univ Lyon, INSA Lyon, Université Claude Bernard Lyon 1, Ecole Centrale de Lyon, CNRS, Ampère, UMR5005
69621 Villeurbanne, France
Email: *laurent.schuller@insa-lyon.fr, †romain.delpoux@insa-lyon.fr, ‡jean-yves.gauthier@insa-lyon.fr, §xavier.brun@insa-lyon.fr

***Abstract*—The synchronous reluctance machine is a promising technology in the electrical machine market. They are now considered in various applications such as transportation or industries. Despite the lack of magnet in such machines, a small residual flux may remains in the ferromagnetic material. This residual flux produces back-electromotive forces as the machine rotates. In this paper, two methods are proposed to determine the back-electromotive forces of the machine online. One is based on the measurements of the short-circuit currents, the other utilizes a linear disturbances observer. The estimations of the back-electromotive forces are then used in the control of the machine in order to compensate their undesirable effects such as current ripples. Both techniques require only the knowledge of the speed and classical electrical parameters of the machine. Experimental results are shown to prove the effectiveness of the proposed approaches.**

***Index Terms*—Synchronous Reluctance machine, Back-Electromotive Forces, ReMa model, disturbances rejection**

I. Introduction

Synchronous Reluctance (SynREL) machines constitute a former technology when it comes to electrical actuators [1]. Because of phase switching and machine design issues, SynREL machines only became a serious competitor in the electrical machines market very recently. These past decades, technological advances in power electronic and computer science have made SynREL machines more effective and novel designs are continuously developed to improve them [2]. SynREL machines are generally three-phase machines, they only differ from others by the particular shape of their rotor, while their stator are highly similar to those of Permanent Magnet Synchronous Machine (PMSM) and Induction Machines (IM) [3]. Although IM have a relatively low efficiency, they are currently the most popular technology in the industrial three-phase electrical machines. However, SynREL machines challenge them [4] both in terms of efficiency and weight [5]. Compared to the PMSM, SynREL machine's performances are definitely inferior. Yet, the excellent performances of PMSM are mainly due to the rare-earth permanent magnet [6] used in such technology. In today's society, theses elements raise several issues in ecological and economical fields [7], [8]. The absence of rare-earth magnet in SynREL machines is a significant advantage. In addition, it allows safer operations of the SynREL machines, in particular if a short circuit appears in the stator winding [9].

Despite the absence of magnet, small back-electromotive forces (EMF) are produced by the residual magnetism of the iron which constitutes the machine [10]. In generator application, these residual magnetic flux, that depend on the magnetic history of the machine, are discussed in [11] [12]. Considering the self start of an isolated SynREL generator, the back-EMF have a paramount importance. Indeed, at low current the back-EMF effect is predominant.

The study of the back-EMF was the subject of a previous work by the authors [13] where a dynamical model of the back-EMF was proposed. However due to the possible changes during the machine operation, it seems useful to propose online solutions to estimate the phenomenon which, to the knowledge of the authors, was never studied.

This article aims to develop two different methods that estimate the back-EMF in order to compensate their unwanted effects: while the first method is based on short-circuit currents measurements, the second one uses a linear observer so as to determine the disturbances caused by the back-EMF. Both methods require only commonly known machine's parameters. Another ambition of this paper is to confront the two proposed methods to the reference ReMa (Residual Magnetism) model presented in [13].

The paper is structured as follows: SynREL technology and dynamical models considering residual magnetism are presented in section II; in section III, the two new methods to determine back-EMF online are detailed and the compensation approach is presented; in section IV experimental results are used to compare both methods to a reference model for small currents, the reduction of the current ripples by compensating the back-EMF is also highlighted. Finally, the conclusion is presented in section V.

II. Model of the SynREL machine

The electrical equations of SynREL machine can be expressed by applying Kirchhoff's voltage law [14] as (1) :

$$\frac{dL(\theta_e)i_{abc}}{dt} = v_{abc} - R_s i_{abc} - e_{abc}, \tag{1}$$

where $i_{abc} = \begin{pmatrix} i_a & i_b & i_c \end{pmatrix}^\intercal$ is the vector of stator currents, $v_{abc} = \begin{pmatrix} v_a & v_b & v_c \end{pmatrix}^\intercal$ is the vector of stator voltages, $e_{abc} = \begin{pmatrix} e_a & e_b & e_c \end{pmatrix}^\intercal$ is the vector of back-EMF on each phase of the machine, θ_e is the electrical position of the rotor, R_s (scalar) is the resistance per phase and $L(\theta_e)$ is the inductance matrix defined as: [1]

$$L(\theta_e) = \begin{pmatrix} L_a & M_{ab} & M_{ca} \\ M_{ab} & L_b & M_{bc} \\ M_{ca} & M_{bc} & L_c \end{pmatrix}, \quad (2)$$

with :

$$\begin{cases} L_a &= L_0 + L_2 cos(2\theta_e), \\ L_b &= L_0 + L_2 cos(2\theta_e + \frac{2\pi}{3}), \\ L_c &= L_0 + L_2 cos(2\theta_e - \frac{2\pi}{3}), \\ M_{ab} &= M_0 + M_2 cos(2\theta_e - \frac{2\pi}{3}), \\ M_{bc} &= M_0 + M_2 cos(2\theta_e), \\ M_{ca} &= M_0 + M_2 cos(2\theta_e + \frac{2\pi}{3}), \end{cases} \quad (3)$$

here, L_0, M_0 and L_2, M_2 are respectively average values and amplitudes of phase inductances and mutual inductances. Leakage inductance have been neglected.

Remark 1. *In this work, back-EMF denote voltages produced when no current flows through the stator windings. Sometimes this term is employed to denominate the voltages generated by the reluctance variations. Depending on currents in each phase, they are not strictly back-EMF from our point of view.*

The back-EMF are generally neglected [14] because of the absence of magnet within the rotor, however, as for most electrical actuators, SynREL machines are mainly made of ferromagnetic materials. The hysteresis property of such materials leads to a small magnetic excitation after being subjected to an intense magnetic field. This results in back-EMF not being zero as modeled in [13]. It results in back-EMF composed of two frequencies in the conventional three-phase frame. The amplitudes and the shapes of the back-EMF depend on the configuration during the magnetizing process, their expressions are given in (4)

$$\begin{cases} e_a &= -\Phi_{rot}\omega_e sin(\theta_e + \delta_0) \\ & \quad -3I_{stat}\omega_e M_2 sin(2\theta_e - \sigma_0), \\ e_b &= -\Phi_{rot}\omega_e sin(\theta_e + \delta_0 - 2\pi/3) \\ & \quad -3I_{stat}\omega_e M_2 sin(2\theta_e - \sigma_0 - 2\pi/3), \\ e_c &= -\Phi_{rot}\omega_e sin(\theta_e + \delta_0 + 2\pi/3) \\ & \quad -3I_{stat}\omega_e M_2 sin(2\theta_e - \sigma_0 + 2\pi/3), \end{cases} \quad (4)$$

where Φ_{rot} and I_{stat} represent the amplitudes of the two frequencies, δ_0 and σ_0 are the direction of the current and the position of the rotor during the magnetization process. Fig. 1 presents an example of simulation results. Unlike IM, the phase-to-phase voltages are not sinusoidal. Indeed, the presence of the second harmonic, due to the residual magnetism within the stator and the reluctance variations, on the phase-to-neutral voltages implies the same second harmonic on the phase-to-phase voltages.

[1]Ignoring the homopolar behavior allows us to consider the hypothesis $M_0 = -\frac{1}{2}L_0$ and $L_2 = M_2$ [15]

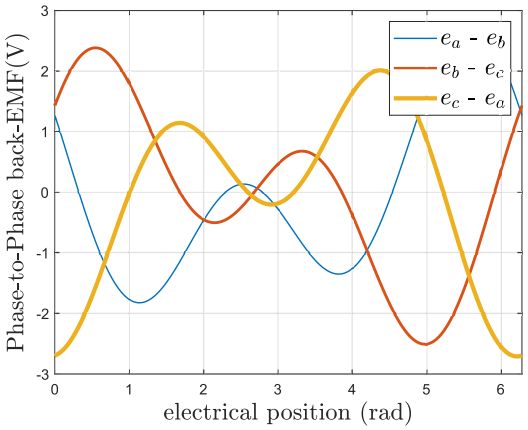

Fig. 1. Simulation of phase-to-phase back-EMF when both the rotor and stator are magnetized. $\omega_e = 209$ rad/s, $M_2 = 0.058$ H, $\Phi_{rot} = 0.0045$ Wb, $I_{stat} = 0.0228$ A, $\sigma_0 = \pi/4$ rad, $\delta_0 = -2\pi/5$ rad

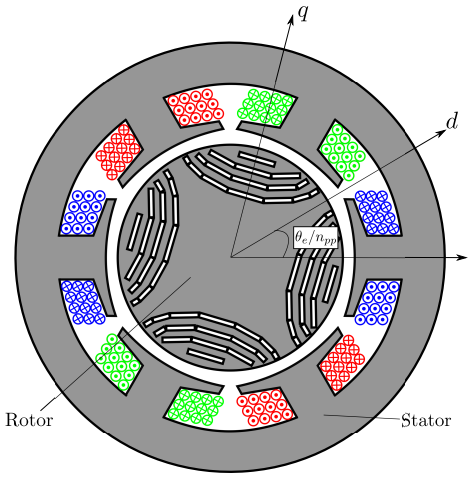

Fig. 2. Schematic cross-section of a SynREL machine with two pole pairs and phase windings (A: blue, B: red, C: green)

Fig. 2 shows a SynREL machine with two pole pairs ($n_{pp} = 2$). The dark areas represent the iron while white parts are made of non-magnetic material such as air. In such machines, the variations of inductances are mainly responsible for the torque generation. The expression of the produced torque is deduced from a power balance (iron losses are neglected) and is expressed as follows:

$$\Gamma_{em} = \frac{1}{2} n_{pp} \left[\frac{\partial L(\theta_e)}{\partial \theta_e} i_{abc} \right]^\intercal i_{abc} + n_{pp} \frac{e_{abc}^\intercal i_{abc}}{\omega_e}, \quad (5)$$

where ω_e is the electrical speed of the machine. The electrical position and speed are linked to their mechanical counterparts (θ_m and Ω_m respectively) by the number of pole pairs: $\theta_e = n_{pp}\theta_m$ and $\omega_e = n_{pp}\Omega_m$. Equation (5) shows that the back-EMF have an impact on the torque generated by the SynREL machine. In particular they can cause undesirable torque ripples.

Because the Park reference frame [16] is very often used to control electric machines, the equivalent dynamical model that takes into account the back-EMF in that frame is given in (6). In the electrical reference frame, the direction of the rotor that involves the maximum of iron is called direction d whereas the so-called q direction is the one with large air-gap (see Fig. 2). With these definitions, the d and q axes are unique and orthogonal in the electrical reference frame. The reference of the electrical position θ_e is chosen such that $\theta_e = 0$ rad coincides with the alignment between the direction d and the phase A windings.

$$L_{dq}\frac{di_{dq}}{dt} = v_{dq} - R_s i_{dq} + \omega_e \mathscr{J} L_{dq} i_{dq} - e_{dq}, \quad (6)$$

with $\mathscr{J} = \begin{pmatrix} 0 & 1 \\ -1 & 0 \end{pmatrix}$. In (6), $L_{dq} = \begin{pmatrix} L_d & 0 \\ 0 & L_q \end{pmatrix}$ is the inductance matrix in the Park frame, v_{dq}, i_{dq} and e_{dq} are respectively the voltages, currents and back-EMF vectors in the Park reference frame. These two back-EMF are composed of a sinusoid p_{x2} with an offset p_{x0} such that $e_d = -p_{d0} - p_{d2}$ and $e_q = -p_{q0} - p_{q2}$ with:

$$\begin{cases} p_{d0} = \omega_e \sqrt{\frac{3}{2}} \Phi_{rot} sin(\delta_0), \\ p_{d2} = 3\sqrt{\frac{3}{2}} I_{stat} \omega_e M_2 sin(\theta_e - \sigma_0), \\ p_{q0} = -\omega_e \sqrt{\frac{3}{2}} \Phi_{rot} cos(\delta_0), \\ p_{q2} = -3\sqrt{\frac{3}{2}} I_{stat} \omega_e M_2 cos(\theta_e - \sigma_0). \end{cases} \quad (7)$$

III. Online determination of the back-EMF

Because the back-EMF may change during the operation of the SynREL machine, the ReMa model is quite sensitive. When the SynREL machine is operating, the back-EMF can not be directly measured. This section aims to develop two different methods for the online determination of the SynREL machine's back-EMF. The estimations of the two proposed methods can be used to compensate the disturbances caused by the back-EMF.

A. Short-circuit currents measurement combined with a Goertzel algorithm

As mentioned previously, there is no problem to short-circuit the stator of a SynREL machine. Indeed, it is even an advantage of this technology compared to the PMSM. During a short-circuit ($v_{abc} = 0$) the equation (1) boils down to:

$$e_{abc} = -\frac{dL(\theta_e)}{dt} i^{sc}_{abc} - L(\theta_e)\frac{di^{sc}_{abc}}{dt} - R_s i^{sc}_{abc} \quad (8)$$

The inductance matrix $L(\theta_e)$ is considered known. Because the back-EMF are composed of only two frequencies, it can be demonstrated that the short-circuit currents contain these same frequencies (considering the remark in the previous footnote [1]). They are hence modeled as follows:

$$i^{sc} = A_0 cos(\theta_e + \Phi_0) + A_2 cos(2\theta_e + \Phi_2), \quad (9)$$

and their derivatives are analytically deduced:

$$\frac{di^{sc}}{dt} = -\omega_e A_0 sin(\theta_e + \Phi_0) - A_2 \omega_e sin(2\theta_e + \Phi_2). \quad (10)$$

To find the parameters present in (9) a Goertzel algorithm is used.

The Goertzel algorithm has been introduced for the first time in 1958 [17]. This algorithm is similar to the discrete Fourier transform applied only for some specific frequencies. Due to its low algorithmic complexity, this method is particularly useful when the number of frequencies is small. For this reason, it has been widely used in fault detection from high frequency injection [18]. The operating details of the algorithm can be found in [19].

From that method, the short-circuit currents derivatives are analytically estimated, thus there is no noise issues. Finally the back-EMF are deduced using (8).

B. Disturbances observer in the Park reference frame

An other method to estimate the back-EMF of the SynREL machine online is presented here. The method is based on a sinusoidal disturbances observer as in [20]. The observer is designed in the Park reference frame. In that frame, the back-EMF are only composed of a constant value and a sinusoidal signal for each axis as presented in (6). The electrical speed ω_e is slowly varying, thus considered constant, so the system is linear. Hence a linear Luenberger observer is designed from the system represented by the following matrix:

$$\begin{cases} \dot{x} = Ax + Bu, \\ y = Cx, \end{cases} \quad (11)$$

with:

$$A = \begin{pmatrix} -\frac{R_s}{L_d} & \omega_e \frac{L_q}{L_d} & \frac{1}{L_d} & 0 & 0 & 0 & \frac{1}{L_d} & 0 \\ -\omega_e \frac{L_d}{L_q} & -\frac{R_s}{L_q} & 0 & 0 & \frac{1}{L_q} & 0 & 0 & \frac{1}{L_q} \\ 0 & 0 & 0 & 1 & 0 & 0 & 0 & 0 \\ 0 & 0 & -\omega_e^2 & 0 & 0 & 0 & 0 & 0 \\ 0 & 0 & 0 & 0 & 0 & 1 & 0 & 0 \\ 0 & 0 & 0 & 0 & -\omega_e^2 & 0 & 0 & 0 \\ 0 & 0 & 0 & 0 & 0 & 0 & 0 & 0 \\ 0 & 0 & 0 & 0 & 0 & 0 & 0 & 0 \end{pmatrix}, \quad (12)$$

$$B = \begin{pmatrix} \frac{1}{L_d} & 0 & 0 & 0 & 0 & 0 & 0 & 0 \\ 0 & \frac{1}{L_q} & 0 & 0 & 0 & 0 & 0 & 0 \end{pmatrix}^\intercal, \quad (13)$$

$$C = \begin{pmatrix} 1 & 0 & 0 & 0 & 0 & 0 & 0 & 0 \\ 0 & 1 & 0 & 0 & 0 & 0 & 0 & 0 \end{pmatrix}, \quad (14)$$

the states of the system are:

$$x = \begin{pmatrix} i_d & i_q & p_{d2} & \dot{p_{d2}} & p_{q2} & \dot{p_{q2}} & p_{d0} & p_{q0} \end{pmatrix}^\intercal, \quad (15)$$

the inputs are:

$$u = \begin{pmatrix} v_d & v_q \end{pmatrix}^\intercal, \quad (16)$$

and the outputs are:

$$y = Cx = \begin{pmatrix} i_d & i_q \end{pmatrix}^\intercal. \quad (17)$$

The observed states ($\widehat{x}$) follow the dynamical equation:

$$\dot{\widehat{x}} = A\widehat{x} + Bu + L_{obs}(y - C\widehat{x}). \quad (18)$$

The gain observer matrix L_{obs} is chosen so that the matrix $(A - L_{obs}C)$ is Hurwitz.

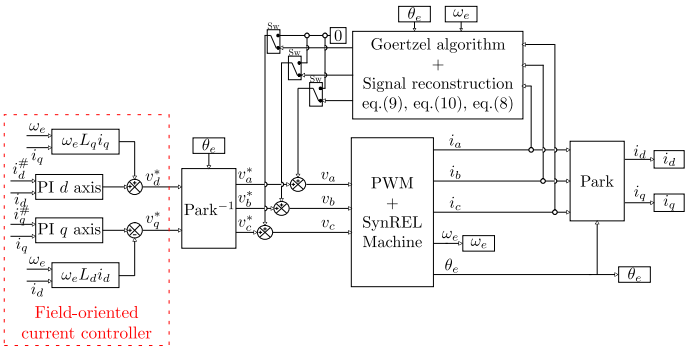

Fig. 3. Control diagram with the first proposed method

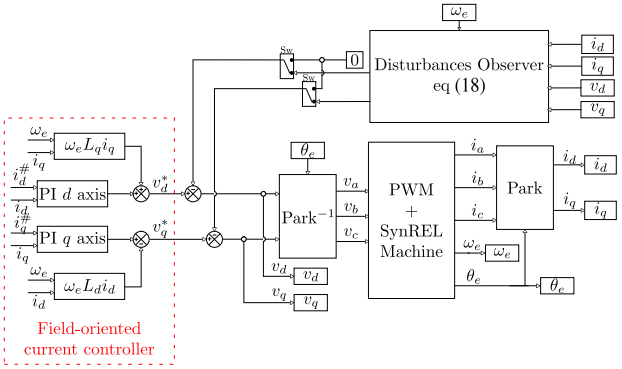

Fig. 4. Control diagram with the second proposed method

This system can not be observed at zero speed. Moreover, some uncertainties, particularly on L_d and L_q may have an effect on the stability of the observer. If the speed varies, a gain scheduling approach may be considered.

C. Feedforward

In [21] the observed disturbances are used to compensate the latter via the inputs of the system. Here, a similar approach is considered. The control diagram is represented on Fig. 3 and Fig. 4 for the two proposed methods.

Thanks to the switch "Sw" the perturbations caused by the back-EMF can either be compensated ("Sw" activated) by the back-EMF estimations or not ("Sw" inactivated).

IV. Experimental results and discussions

In this section the experimental results are presented. The different methods are analyzed and compared to each other.

A. Description of the test bench

For the experimental tests, a BSR90LE154055FB5 SynREL machine from Bonfigioli is used. Its main characteristics are listed in Table I. A Leroy-Somer 95UMC300HAAAA PMSM with the same speed and power range is attached to the SynREL machine by the shafts. Both machines are fed through three-phase inverters composed of NTHL080N120SC1 SiC MOSFET. Position and speed measurements are provided by an incremental encoder with 5000 points per mechanical revolution. All acquisitions are extracted through a dSpace MicroLabBox Rapid Control Prototyping (RCP) System. The experimental setup is presented in Fig. 5.

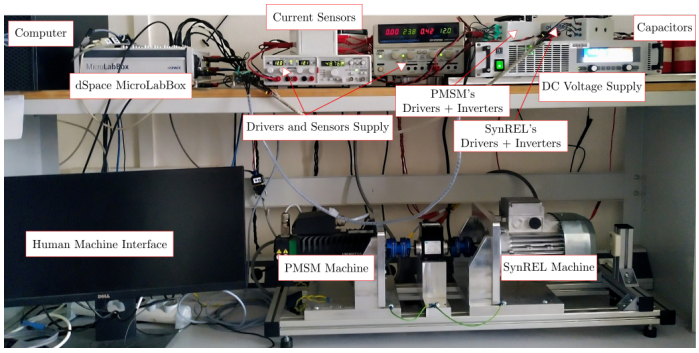

Fig. 5. Experimental setup

A classical current vector control combined with a Proportional-Integral (PI) speed controller is used to drive the PMSM machine at a constant speed. The PIs of the field-oriented current controllers of the SynREL machine are chosen such that the closed loop dynamic response is the same for the both axis and the controllers are the same for all the experiments.

TABLE I
Main Parameters of the Synchronous Reluctance Machine

Parameters	Value	Units
Base speed (mechanical) Ω_m	157	rad/s
Number of pole pairs n_{pp}	2	$-$
Rated current I_n	4.5	A
Power P_n	1500	W
Nominal phase voltage V_n	230	V
Resistance per phase R_s	2.6	Ω
Unsaturated inductance amplitude L_2	0.078	H
Unsaturated inductance average value L_0	0.144	H
Unsaturated Mutual amplitude M_2	0.058	H
Unsaturated Mutual average value M_0	-0.048	H
Unsaturated d-axis inductance L_d	0.289	H
Unsaturated q-axis inductance L_q	0.095	H

B. Experimental back-EMF determination

1) Estimated back-EMF: the PMSM is driven so that the mechanical speed is kept constant. The SynREL machine is in a first time short-circuited and no feedforward compensation is considered ("Sw" inactivated). The short-circuit is accomplished by imposing the same constant duty-cycle on each phase of the inverter-fed machine. Despite the potential dead-time effect, it was experimentally verified that the behavior was the same as with a real short-circuit. During this, the Goertzel algorithm method is applied in order to determine the back-EMF from this first method. The identified parameters are stored in memory in order to be used hereafter. After that, the SynREL machine is controlled to regulate the current at zero. There is still no feedforward compensation ("Sw" inactivated). The Observed back-EMF are computed and another estimation of these latter is then available.

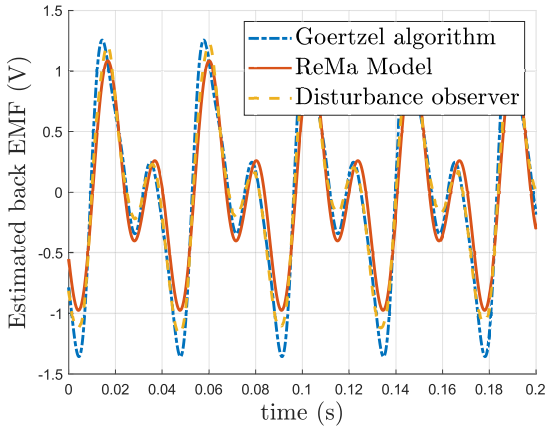

Fig. 6. Comparison of the two proposed methods and the ReMa model ($\Omega_m = 72.2$ rad/s)

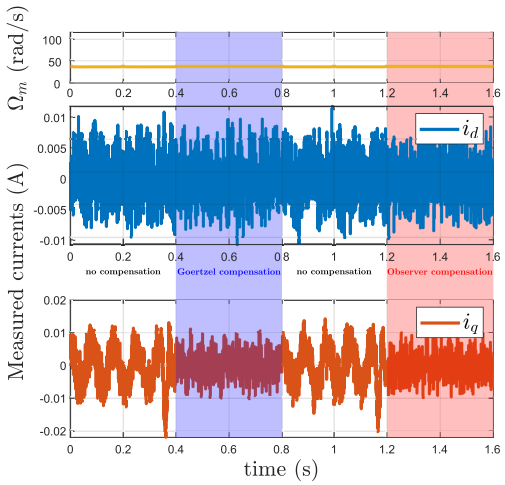

Fig. 7. Current measurements for different compensations of the back-EMF ($\Omega_m = 36.6$ rad/s)

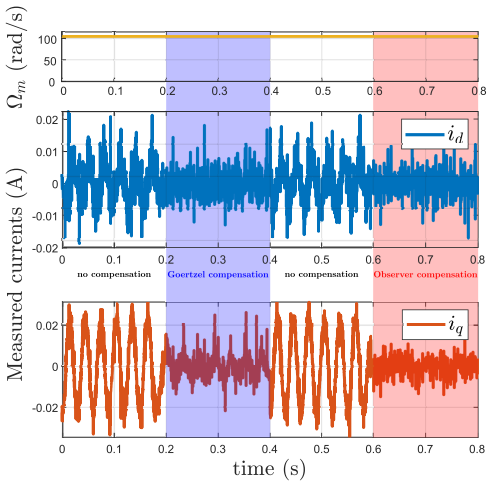

Fig. 8. Current measurements for different compensations of the back-EMF ($\Omega_m = 105$ rad/s)

On the figure Fig. 6 the two proposed methods results are compared to the ReMa model [13] on phase A for a constant mechanical speed of 72.2 rad/s. The two procedures provide satisfactory results both in term of shape and amplitude although the observer method is slightly better than the Goertzel algorithm based method. The similarity of the results make us more confident on the estimation of the back-EMF.

2) back-EMF compensation: the feedforward compensation is now considered. The estimated back-EMF are used to compensate the current ripples caused by the back-EMF. Again the PMSM is driven so that the mechanical speed is kept constant. The SynREL machine is controlled to keep its currents at zero. While the observer's estimated back-EMF are computed online, those of Goertzel's algorithm are based on the previous short-circuit process. The currents i_d and i_q are measured for different compensation methods as shown on Fig. 7 and Fig. 8.

The performances of the estimation methods are deduced from the efficiency of the disturbance compensation. Although visible for the direct current i_d, the effect of the back-EMF compensation is particularly notable on i_q. This is due to the fact that the disturbances are bigger on the q axis than in the direct one because of the lower value of the inductance L_q compared to L_d. On Fig. 7 the two proposed methods provide similar results. However, the methods implying a Goertzel algorithm consumes more computational resources. This algorithmic complexity may be improved by deducing the three currents from only one measured using the classical relations between the currents.

The effects of the disturbances compensation is even better when the speed increases since the higher the speed, the bigger the disturbances. Furthermore, when the disturbances frequency increases, the natural disturbances rejection of the PI current controllers is less and less effective.

Fig. 8 shows the results for the back-EMF compensation methods when the machine rotates at a mechanical speed of 105 rad/s.

On that figure the effect of the compensation is visible for both axes. The compensation from the observer method provides better results. However, the methods based on the Goertzel algorithm has no risk of instability and is easier to tune. Indeed, depending on the required frequency resolution, a simple relation relies sample frequency and the measure duration. While the choice of L_{obs} matrix is no that trivial.

3) Perspectives: it is commonly accepted that the residual magnetism can change during operation. To confirm this, the back-EMF are observed for different current loads while the PMSM makes the SynREL machine rotate at a constant speed. No back-EMF compensation is considered here ("Sw" inactivated). Starting from a regulation of the i_d and i_q currents at zero. A current step is generated by imposing $i_d = i_q = 1.5$ A. After that the currents are once again regulated to zero.

The Fig. 9 shows the back-EMF (in the three-phase frame) on phase A observed by the second method for the described operations of the SynREL machine. From that figure, it can be

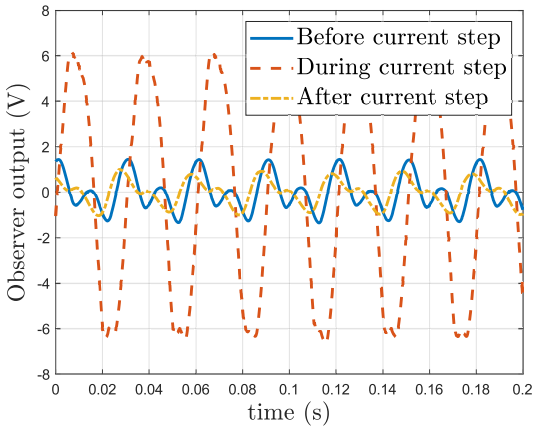

Fig. 9. Observed back-EMF for different operations

seen that the back-EMF change depending on the history of the machine. The ReMa model, that does not change online, is close to the solid line of Fig. 9 as proved on Fig. 6. However, after applying a current step on both d and q axis, the back-EMF change. When currents are flowing through the stator windings, the back-EMF are over estimated. Indeed, during such operation, the inductance L_q and more likely L_d can saturate. This generates errors in our model, these errors on the inductances are included into the observed perturbations. For such cases, the estimation of the back-EMF can be improved by taking into account the saturation of the inductances. More generally the both proposed methods are sensitive to inductances variations. This latter point is suggested as a further work to improve the present development.

V. Conclusion

Two methods to determinate the back-Electromotive forces of a SynREL machine online are presented in this paper. The two suggested strategies require only commonly known machine's parameters. The first proposed method is based on a short-circuit currents measurement. The second approach relies on a linear disturbances observer in the Park reference frame. The estimations of the two proposed methods can be used to compensate the disturbances caused by the back-EMF. Both methods are compared to a previously developed ReMa model of the SynREL machine. The experimental results show that both methods are effective to estimated the back-EMF of the SynREL machine. Experiments show good results for the compensations at low currents. Making the compensation more efficient at higher currents is a considered perspective that certainly requires a more precise inductance model.

References

[1] J. Kostko, "Polyphase reaction synchronous motors," *Journal of the American Institute of Electrical Engineers*, vol. 42, no. 11, pp. 1162–1168, 1923.

[2] Y. Bao, M. Degano, S. Wang, L. Chuan, H. Zhang, Z. Xu, and C. Gerada, "A novel concept of ribless synchronous reluctance motor for enhanced torque capability," *IEEE Transactions on Industrial Electronics*, vol. 67, no. 4, pp. 2553–2563, 2020.

[3] C. Donaghy-Spargo, "Synchronous reluctance motor technology: opportunities, challenges and future direction." *Engineering & technology reference.*, pp. 1–15, 2016.

[4] A. Boglietti and M. Pastorelli, "Induction and synchronous reluctance motors comparison," in *2008 34th Annual Conference of IEEE Industrial Electronics*, 2008, pp. 2041–2044.

[5] A. Rassolkin, H. Heidari, A. Kallaste, T. Vaimann, J. P. Acedo, and E. Romero-Cadaval, "Efficiency map comparison of induction and synchronous reluctance motors," in *2019 26th International Workshop on Electric Drives: Improvement in Efficiency of Electric Drives (IWED)*. IEEE, 2019, pp. 1–4.

[6] M. A. Rahman, "History of interior permanent magnet motors [history]," *IEEE Industry Applications Magazine*, vol. 19, no. 1, pp. 10–15, 2012.

[7] T. Jahns, "Getting rare-earth magnets out of ev traction machines: A review of the many approaches being pursued to minimize or eliminate rare-earth magnets from future ev drivetrains," *IEEE Electrification Magazine*, vol. 5, no. 1, pp. 6–18, 2017.

[8] I. Boldea, L. N. Tutelea, L. Parsa, and D. Dorrell, "Automotive electric propulsion systems with reduced or no permanent magnets: An overview," *IEEE Transactions on Industrial Electronics*, vol. 61, no. 10, pp. 5696–5711, 2014.

[9] D. Qin, X. Luo, and T. Lipo, "Reluctance motor control for fault-tolerant capability," in *1997 IEEE International Electric Machines and Drives Conference Record*. IEEE, 1997, pp. WA1–1.

[10] Y. Wang and N. Bianchi, "Investigation of self-excited synchronous reluctance generators," *IEEE Transactions on Industry Applications*, vol. 54, no. 2, pp. 1360–1369, 2017.

[11] M. Ibrahim and P. Pillay, "The loss of self-excitation capability in stand-alone synchronous reluctance generators," *IEEE Transactions on Industry Applications*, vol. 54, no. 6, pp. 6290–6298, 2018.

[12] S. S. Maroufian and P. Pillay, "Self-excitation criteria of the synchronous reluctance generator in stand-alone mode of operation," *IEEE Transactions on Industry Applications*, vol. 54, no. 2, pp. 1245–1253, 2017.

[13] L. Schuller, J.-Y. Gauthier, R. Delpoux, and X. Brun, "Dynamical Model of Residual Magnetism for Synchronous Reluctance Machine Control," Jun. 2021, working paper or preprint. [Online]. Available: https://hal.archives-ouvertes.fr/hal-03255256

[14] S. E. Lyshevski, A. Nazarov, A. El-Antably, A. Sinha, M. Rizkalla, and M. El-Sharkawy, "Synchronous reluctance motors: nonlinear analysis and control," in *Proceedings of the 2000 American Control Conference. ACC (IEEE Cat. No. 00CH36334)*, vol. 2. IEEE, 2000, pp. 1108–1112.

[15] A. Chiba, F. Nakamura, T. Fukao, and M. A. Rahman, "Inductances of cageless reluctance-synchronous machines having nonsinusoidal space distributions," *IEEE Transactions on Industry Applications*, vol. 27, no. 1, pp. 44–51, 1991.

[16] R. H. Park, "Two-reaction theory of synchronous machines generalized method of analysis-part i," *Transactions of the American Institute of Electrical Engineers*, vol. 48, no. 3, pp. 716–727, 1929.

[17] G. Goertzel, "An algorithm for the evaluation of finite trigonometric series," *The American Mathematical Monthly*, vol. 65, no. 1, pp. 34–35, 1958.

[18] F. Briz, M. W. Degner, A. B. Diez, and J. M. Guerrero, "Online diagnostics in inverter-fed induction machines using high-frequency signal injection," *IEEE Transactions on Industry Applications*, vol. 40, no. 4, pp. 1153–1161, 2004.

[19] E. Najafi and A. Yatim, "A novel current mode controller for a static compensator utilizing goertzel algorithm to mitigate voltage sags," *Energy Conversion and Management*, vol. 52, no. 4, pp. 1999–2008, 2011.

[20] A. A. Godbole, J. P. Kolhe, and S. E. Talole, "Performance analysis of generalized extended state observer in tackling sinusoidal disturbances," *IEEE Transactions on Control Systems Technology*, vol. 21, no. 6, pp. 2212–2223, 2012.

[21] F. P. Scalcon, T. S. Gabbi, R. P. Vieira, and H. A. Gründling, "Decoupled vector control based on disturbance observer applied to the synchronous reluctance motor," in *2019 21st European Conference on Power Electronics and Applications (EPE'19 ECCE Europe)*. IEEE, 2019, pp. P–1.